

# Self-Testing Mutually Unbiased Bases in Higher Dimensions with Space-Division Multiplexing Optical Fiber Technology

Máté Farkas<sup>1,2,3</sup>, Nayda Guerrero<sup>4,5</sup>, Jaime Cariñe<sup>6,5</sup>, Gustavo Cañas<sup>7,\*</sup>, and Gustavo Lima<sup>4,5</sup>

<sup>1</sup>*Institute of Theoretical Physics and Astrophysics, National Quantum Information Center, Faculty of Mathematics, Physics and Informatics, University of Gdańsk, 80-952 Gdańsk, Poland*

<sup>2</sup>*International Center for Theory of Quantum Technologies, University of Gdańsk, 80-308 Gdańsk, Poland*

<sup>3</sup>*ICFO—Institut de Ciències Fotoniques, The Barcelona Institute of Science and Technology, 08860 Castelldefels Barcelona, Spain*

<sup>4</sup>*Departamento de Física, Universidad de Concepción, 160-C Concepción, Chile*

<sup>5</sup>*Millennium Institute for Research in Optics, Universidad de Concepción, 160-C Concepción, Chile*

<sup>6</sup>*Departamento de Ingeniería Eléctrica, Universidad Católica de la Santísima Concepción, Concepción, Chile*

<sup>7</sup>*Departamento de Física, Universidad del Bío-Bío, Collao 1202, Casilla 5C, Concepción, Chile*



(Received 11 June 2020; revised 15 November 2020; accepted 15 December 2020; published 15 January 2021)

In the device-independent quantum-information approach, the implementation of a given task can be self-tested solely from the recorded statistics and without detailed models for the employed devices. Even though experimentally demanding, it provides appealing verification schemes for advanced quantum technologies that naturally fulfil the associated requirements. In this work, we experimentally study whether self-testing protocols can be adopted to certify the proper functioning of quantum devices built with modern space-division multiplexing optical fiber technology. Specifically, we consider the prepare-and-measure protocol of Farkas and Kaniewski [Phys. Rev. A 99, 032316 (2019)] for self-testing measurements corresponding to mutually unbiased bases (MUBs) in a dimension  $d > 2$ . In our scheme, the state preparation and measurement stages are implemented using a multiarm interferometer built with multicore optical fibers and related components. Due to the high overlap of the interferometer's optical modes achieved with this technology, we are able to reach the required visibilities for self-testing the implementation of two four-dimensional MUBs. We also quantify two operational quantities of the measurements: (i) the incompatibility robustness, connected to Bell violations, and (ii) the randomness extractable from the outcomes. Since MUBs lie at the core of several quantum-information protocols, our results are of practical interest for future quantum works relying on space-division multiplexing optical fibers.

DOI: 10.1103/PhysRevApplied.15.014028

## I. INTRODUCTION

The advent of quantum-information technologies comes with promises such as exponential computational speed-up compared to currently existing classical algorithms [1,2] or unconditionally secure quantum communication [3,4]. However, the success of these protocols relies on certification methods to verify that the used devices perform the tasks they are promised to perform. Furthermore, it should be possible to perform these verification methods efficiently and using only classical resources. Consequently, they are currently the subject of intensive study in the quantum-information community [5–12], where they are commonly referred to as self-testing protocols. The strongest method is known as the “device-independent

approach,” which involves two parties sharing an entangled quantum state, and the only considered assumption for self-testing the proper implementation of a given task is that these parties are spacelike separated. The certification is based solely on the recorded measurement statistics of the two parties [13]. This method, however, comes with a few drawbacks. First, it is rather challenging to implement experimentally, as it requires the production of entangled states with very high fidelities. Second, in dimensions larger than two, the theoretical treatment becomes complex as well. Accordingly, there are only a few theoretical results available for high-dimensional quantum states (qudits) [14,15] and the method has never been experimentally demonstrated.

Nonetheless, the use of qudit systems is advantageous for several quantum-information tasks. For example, they allow for larger violations of Bell inequalities [16],

\*gustavocanascardona@gmail.com

improvement on quantum computation and communication complexity tasks [17,18], and higher randomness-generation rates [19]. Thus, there is a current need for more practical self-testing protocols in higher dimensions. In order to alleviate the difficulties mentioned above, several relaxations of the demanding device-independent scheme have been introduced. One generic direction is to move to the experimentally less demanding prepare-and-measure scenario, in which instead of sharing an entangled state, one party prepares a state and sends it to the other party, who then measures it. In this scenario, further reasonable assumptions are necessary to devise certification methods. These include bounds on the average energy of the quantum states [20] or the indistinguishability of the different states prepared [21]. Perhaps the most traditional such relaxation is to fix the dimension of the quantum states [6,22–24].

Recently, in Ref. [25], a method has been proposed for self-testing high-dimensional measurements corresponding to mutually unbiased bases (MUBs) in the prepare-and-measure scenario, under the dimension assumption. MUBs constitute a particularly useful family of quantum measurements, with myriad applications in quantum information. Among other tasks, they optimize state determination [26,27], generate the maximal amount of randomness [28], and give rise to secure cryptographic protocols [3] (for a survey, see Ref. [29]). The authors of Ref. [25] anticipate that their certification method can be performed with currently available technologies in dimensions larger than two. This is precisely the aim of the current work, in which we experimentally study whether self-testing certification methods can be adopted in the platform of space-division multiplexing (SDM) optical fiber technology to quantum-information processing [30]. In our scheme, we use single-photon path-encoded four-dimensional quantum systems (ququarts) and the state preparation and measurement stages are implemented by resorting to an advanced four-arm interferometer built of multicore optical fibers and related technology, which we present next. As observed in Ref. [19], this scheme should, in principle, attain the optical quality required for implementing self-testing protocols. Indeed, here, in our test of Ref. [25], we are able to record the corresponding data with an average visibility of  $99.89 \pm 0.03\%$ , which allows us to self-test the proper implementation of a pair of four-dimensional MUBs. Moreover, we also certify the incompatibility of our implemented measurements and the randomness extractable from their outcomes. Note that while this same type of protocol has already been implemented experimentally in higher dimensions [31–34], the error rates have never been suppressed to a level that would allow the self-testing of the measurements performed.

Our results highlight the advantages of modern SDM technologies for high-dimensional quantum-information processing, by demonstrating that devices based on this

technology can be self-tested. This means that state preparations and measurements can be performed on this platform with very high fidelity. Furthermore, the self-tested MUB measurements are widely useful in quantum-information processing, proving this technology to be of broad relevance in the field. Lastly, we note that the self-testing protocol adopted can be regarded as a generalization of the quantum key distribution protocol of Ref. [35].

## II. THEORY

Formally, a pair of MUBs in dimension  $d$  corresponds to two rank-1 measurements projecting onto the orthonormal bases  $\{|a_i\rangle\}_{i=1}^d$  and  $\{|b_j\rangle\}_{j=1}^d$  on  $\mathbb{C}^d$ . We say that these bases are mutually unbiased if

$$|\langle a_i | b_j \rangle|^2 = \frac{1}{d} \quad \forall i, j \in \{1, \dots, d\}, \quad (1)$$

that is, every pair of vectors from different bases has the same overlap. One simple example is the eigenbases of the Pauli  $X$  and  $Z$  operators on a qubit.

The prepare-and-measure self-testing method used in Ref. [25] to certify  $d$ -dimensional MUB measurements is based on the so-called  $2^d \rightarrow 1$  quantum-random-access-code (QRAC) protocol. In a QRAC, the preparation side (Alice) receives two uniformly random classical dits,  $i, j \in \{1, \dots, d\}$ . Based on this input, Alice prepares the  $d$ -dimensional quantum state,  $\rho_{ij}$ , and sends it to Bob on the measurement side. Bob receives a uniformly random classical bit,  $y \in \{1, 2\}$ , based on which he decides which observable to measure on the state  $\rho_{ij}$ . If  $y = 1$ , his measurement is a  $d$ -outcome positive-operator-valued measure (POVM), the measurement operators of which are denoted by  $A_i$ . Similarly, for  $y = 2$ , he measures  $B_j$ . Recall that for POVMs we have that  $A_i, B_j \geq 0$  and  $\sum_{i=1}^d A_i = \sum_{j=1}^d B_j = \mathbb{I}$ . That is, a  $d$ -outcome POVM is a set of  $d$  positive semidefinite operators that add up to the identity operator. Let us denote the outcome of Bob's measurement by  $b \in \{1, \dots, d\}$ . The common aim of the parties is that when  $y = 1$ , Bob's output equals Alice's first input, that is,  $b = i$ , and when  $y = 2$ , they have  $b = j$ . To quantify their success rate, we employ the *average success probability* (ASP)  $\bar{p} = \frac{1}{2} [P(b = i | y = 1) + P(b = j | y = 2)]$  as the figure of merit. According to the Born rule, the probability of Bob outputting  $b$  when Alice's input is  $i, j$  and Bob's input is  $y = 1$  is  $\text{tr}(\rho_{ij} A_b)$  and, similarly, it is  $\text{tr}(\rho_{ij} B_b)$  when  $y = 2$ . That is, the ASP for a generic encoding scheme  $\rho_{ij}$  and measurement choice  $A_i$  and  $B_j$  can be written as

$$\bar{p} = \frac{1}{2d^2} \sum_{i,j=1}^d \text{tr} [\rho_{ij} (A_i + B_j)]. \quad (2)$$

In Ref. [25], the authors provide certificates for MUBs based only on the recorded ASP in a QRAC. They show that in dimension  $d$ ,  $\bar{p} \leq \frac{1}{2}(1 + 1/\sqrt{d}) =: \bar{p}_Q$  and this maximum can only be attained if Bob's measurements correspond to a pair of MUBs. Moreover, even for suboptimal  $\bar{p}$ , one can certify the closeness of the employed measurements to a pair of MUBs. Specifically, one can bound the entropy of the generalized overlaps of the two measurements and the sum of the individual operator norms. These two measures together—having sufficiently high values—imply that the measurement operators have close-to-uniform overlaps and are close to being rank-1 projectors, that is, they are close to MUBs.

Specifically, the first quantity employed is the *overlap entropy*,  $H_S(A, B) = H_{\frac{1}{2}} \left\{ [\text{tr}(A_i B_j)/d]_{ij} \right\}$ , where  $H_{1/2}$  is the  $\frac{1}{2}$ -Rényi entropy [note that for projective measurements,  $\text{tr}(A_i B_j) = |\langle a_i | b_j \rangle|^2$ ]. It has been shown that given an observed ASP  $\bar{p}$ , it holds for the measurements  $A$  and  $B$  that [25]

$$H_S(A, B) \geq 2 \log \left[ d\sqrt{d}(2\bar{p} - 1) \right]. \quad (3)$$

The maximal possible value of the overlap entropy,  $\log d^2$ , is reached by MUBs and can be certified upon observing  $\bar{p} = \bar{p}_Q$ .

The second quantity is the *sum of the norms*,  $N(A) = \sum_{i=1}^d \|A_i\|$ . It has also been shown in Ref. [25] that

$$N(A) \geq d - \frac{2 + \sqrt{2}}{d} \left[ 1 - \sqrt{d^3(2\bar{p} - 1)^2 - (d^2 - 1)} \right], \quad (4)$$

and the same holds for  $B$ . The maximal possible value of the sum of the norms,  $d$ , is reached if and only if the measurements are rank-1 projective and this can be certified upon observing  $\bar{p} = \bar{p}_Q$ .

Putting the above two bounds together, observing  $\bar{p} = \bar{p}_Q$  implies that  $\text{tr}(A_i B_j) = 1/d$  for all  $i, j$  and that the measurements are rank-1 projective. In other words,  $\bar{p} = \bar{p}_Q$  certifies that Bob's measurements correspond to a pair of MUBs. By the continuity of the bounds in  $\bar{p}$ , it follows that if the observed ASP is suboptimal,  $\bar{p} < \bar{p}_Q$ , but close to optimal, then the overlap entropy and the sum of the norms are both close to their unique MUB values. This serves as a certificate that the employed measurements are close to MUBs.

Lastly, the authors of Ref. [25] derive certificates for two useful properties of the measurements: incompatibility robustness and the amount of randomness generated. The former, briefly speaking, is the maximal visibility of the measurements at which they are jointly measurable (compatible) [36]. Clearly, for compatible measurements pairs, this maximal visibility is 1 and the lower the value, the

more incompatible the pair is. Jointly measurable observables are of no use in nonlocal and steering scenarios [37] and therefore it is important to quantify the extent to which a pair of measurements is incompatible. In Ref. [25], the authors show that the incompatibility robustness of  $A$  and  $B$  is bounded by

$$\eta^* \leq \frac{\frac{1}{2}d^2(1 + s_{\max}) - \frac{N(A)^2}{d}}{N(A)^2 - d - [d - N(A)][d - N(A) + 1]}, \quad (5)$$

where  $s_{\max} = \max_{ij} \|\sqrt{A_i} \sqrt{B_j}\|$ . Using the bounds in Eqs. (3) and (4), one can then bound the incompatibility robustness by the observed ASP. The value corresponding to a pair of MUBs,  $\eta^* = \frac{1}{2} \left[ 1 + 1/(\sqrt{d} + 1) \right]$ , can be certified upon observing  $\bar{p} = \bar{p}_Q$ .

The second quantity to certify is the amount of uncertainty produced in the outcome of the measurements, formulated as an entropic uncertainty relation [38]. This amounts to a lower bound on the entropy of the measurement outcome probabilities in a state-independent fashion. Let us denote the Shannon entropy of the outcome probabilities of the measurement  $A$  on the state  $\rho$  by  $H(A)_\rho$ . Then, it has been shown in Ref. [25] that given a QRAC ASP  $\bar{p}$ , it holds that

$$H(A)_\rho + H(B)_\rho \geq -2 \log \left( 2\bar{p} - 1 + \frac{1}{d} \sqrt{d(d^2 - 1)[1 - d(2\bar{p} - 1)^2]} \right), \quad (6)$$

for any state  $\rho$ . Note that the maximal value for rank-1 projective measurements,  $\log d$ , can again be certified upon observing  $\bar{p} = \bar{p}_Q$ .

### III. SPACE-DIVISION MULTIPLEXING TECHNOLOGY

SDM is a classical telecommunication technique that uses multiple transverse optical modes for increasing data-communication capacity. The SDM technique is implemented for optical communication links in both free space and fiber optics [39,40]. It is considered a crucial solution to overcome the so-called “capacity crunch” of fiber-optic communications [40]. In this case, SDM technology is typically based on few-mode fibers (FMFs) [41–43], ring-core fibers (RCFs) [44], and multicore fibers (MCFs) [45,46]. These are schematically represented in Fig. 1.

FMFs are a particular class of multimode fibers (MMFs), which support only a few linearly polarized transverse optical modes [41–43]. Each mode that is supported in a FMF has very low crosstalk to the others and, therefore, can be used as an independent data channel. RCFs are optical fibers with an annular refractive index profile that supports multiple Laguerre-Gaussian beams

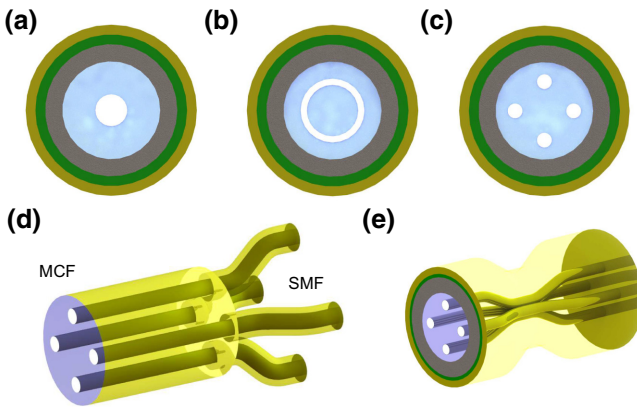


FIG. 1. The fibers and components typically used in the SDM approach for fiber-optics communication. A schematic representation of the cross section of (a) a few-mode fiber, (b) a ring-core fiber, and (c) a multicore fiber (with four cores). Each of them is composed of a core (white), cladding (light blue), a coating (gray), a strength member (green), and an outer jacket (yellow). A FMF supports the propagation of a few linearly polarized modes. A RCF has an annular core that supports, for instance, the propagation of some Laguerre-Gaussian optical modes. The MCF is a single fiber with several single-mode cores within its cladding. (d) The schematics of demultiplexer devices used for efficiently coupling light into multicore fibers (insertion loss  $<0.7$  dB). (e) An example of a four-core fiber-integrated multiport beam splitter.

carrying orbital angular momentum (OAM) [47]. Lastly, there are MCFs, which are considered to be the most promising solution for SDM, since their fabrication is cost effective [46]. An MCF is a single fiber containing multiple cores within the same cladding, which are sufficiently separated from each other to avoid light coupling between them. Typically, crosstalk between the cores is negligible with more than 60 dB of attenuation [46].

Together with the development of these fibers, several related components have been built to improve the efficiency of SDM techniques. For instance, there are multiplexer-demultiplexer (DEMUX) devices, used to combine and separate the different transverse optical modes supported by the SDM fiber. Typically, these devices have  $N$  independent single-mode fibers connected to the SDM fiber, mapping  $N$  transverse Gaussian modes onto the  $N$  particular optical modes supported by the SDM fiber. For FMFs, DEMUXs called photonic lanterns are used [48]. For RCFs, these devices are called mode sorters. They are usually built with bulk optics [49] but an important recent development is an all-fiber mode sorter [50]. Finally, the DEMUXs used for MCFs are devices composed of single-mode fibers (SMFs), each one connected to one core of the MCF. These devices are already commercially available and are built using a fiber-bundle polishing-and-tapering technique, presented

in Refs. [51,52]. In Fig. 1(d), we show, as an example, the schematics of a MCF DEMUX.

Our experimental setup is based on MCFs and in this case another important device is the multicore fiber-integrated multiport beam splitter (MBS), recently presented in Ref. [19] [see Fig. 1(e)]. This device is crucial for quantum-information processing because it allows one to implement distinct unitary operations representing the change of basis from the logical basis to a basis that is mutually unbiased to it. Thus, it allows for the generation and measurement of a general class of quantum states, as we explain in the next section. The MBS is fabricated directly within a multicore fiber, using a tapering technique for MCFs [53]. By tapering the fiber, the cores are brought together and, due to evanescent effects, there is light coupling from one core to the others. Due to the symmetry of the MCF structure, the splitting ratio can be made balanced for all core-to-core combinations.

#### IV. EXPERIMENT

Recently, the technology developed for SDM has become a platform for high-dimensional quantum-information processing [30]. Initial efforts, based on path-encoded qudits and multicore fibers [54–58], have now been expanded to different types of fibers and encoding schemes [59–62]. Nonetheless, this platform has not yet been demonstrated to be compatible with modern self-testing protocols of quantum states and circuits. Here, we fill this gap by extensively studying the protocol of Ref. [25]. Specifically, we measure the QRAC ASP and bound all the quantities of Eqs. (3)–(6) with a four-arm Mach-Zehnder (MZ) interferometer built of MCFs and the related technology discussed above.

The state preparations in the QRAC protocol are realized by photonic states. The initial photon source is a continuous-wave telecom laser, operating at 1546 nm (see Fig. 2). It is connected to an external fiber-pigtailed amplitude modulator (FMZ), which is controlled by a field-programmable gate array (FPGA) electronic unit to generate 5-ns-wide pulses. Then, we use optical attenuators (ATT) to create weak coherent states. The attenuators are calibrated to set the average number of photons per pulse to  $\mu = 0.2$ . In this case, the probability of having pulses containing at least one photon is  $P(n \geq 1|\mu = 0.2) \approx 18\%$ . Most of the non-null pulses contain only one photon and represent 90.3% of the experimental runs. Therefore, our source can be seen as a good approximation of a non-deterministic source of single photons [63]. We note that coincidence detections are not discarded in our analysis and that the proportion of events where coincidence detections occurs is much smaller than 1.81%. It corresponds to only 0.045%, which is a consequence, for instance, of the fact that, in some cases, both photons go to the same

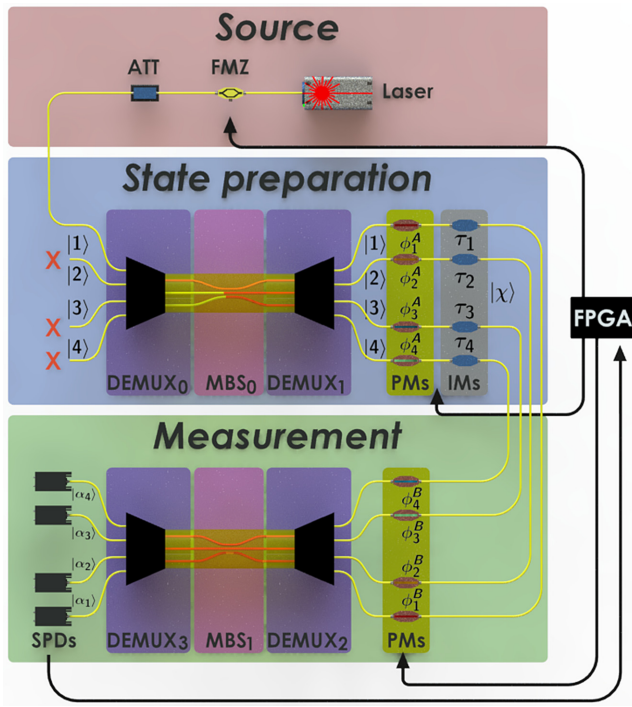


FIG. 2. The experimental setup is based on a four-arm Mach-Zehnder interferometer built of four-core multicore fibers (MCF) and related technology (see Sec. III). The interferometer is used for preparing and measuring path-encoded ququart states. At the state-preparation stage, the initial state is prepared by a set composed of a  $4 \times 4$  MCF based multiport beam splitter (MBS<sub>0</sub>) and phase (PM) and amplitude (IM) fiber-pigtailed modulators. The measurement is achieved using another set of PMs and a second MBS<sub>1</sub> connected to four single-photon detection (SPD) modules. The field-programmable gate array (FPGA) electronic unit automatically controls the protocol implementation. See the main text for details.

detector—or to the more general fact that, in most of the cases, one photon is detected and the other is not.

The signal from the source is sent to a commercial-fiber built-in DEMUX unit (DEMUX<sub>0</sub>), which consists of four independent single-mode fibers, each of them connected to one core of a four-core MCF. The source is connected through one of the four SMFs of DEMUX<sub>0</sub>; therefore, only one core of the MCF is illuminated. DEMUX<sub>0</sub> is then connected to a MCF-based  $4 \times 4$  MBS (denoted MBS<sub>0</sub>), the matrix representation of which is given by [19]

$$U_{\text{MBS}} = \frac{1}{2} \begin{bmatrix} 1 & 1 & 1 & 1 \\ 1 & 1 & -1 & -1 \\ 1 & -1 & 1 & -1 \\ 1 & -1 & -1 & 1 \end{bmatrix} \quad (7)$$

in the logical basis. In our scheme, the logical states are defined in terms of the core modes available for the photon propagation over the multicore fiber [19,55]. Therefore, the

$4 \times 4$  MBS corresponds to a Hadamard gate in dimension four.

MBS<sub>0</sub> is then coupled to a second DEMUX (denoted DEMUX<sub>1</sub>) via their respective MCFs. In order to control the initial quantum state entering the interferometer, we connect phase (PM) and amplitude (IM) fiber-pigtailed modulators to each SMF of DEMUX<sub>1</sub>, these being controlled by the FPGA. The general path-encoded ququart state that we can prepare in the first part of the MZ is then given by

$$|\chi\rangle = \frac{1}{\sqrt{N}} \sum_{k=1}^4 \tau_k e^{i\phi_k^A} |k\rangle, \quad (8)$$

where  $|k\rangle$  represents the state of the photon transmitted in the  $k$ th core (i.e., the  $k$ th logical state).  $\tau_k$  and  $\phi_k^A$  are the transmissivity and relative phase, respectively, of core  $k$  and  $N$  is the normalization constant.

Having prepared the state, the measurements are performed in a similar fashion, using a second set of PMs, DEMUX<sub>2</sub> and MBS<sub>1</sub> [19]. The resulting unitary operation implemented is

$$U_M = \frac{1}{2} \begin{bmatrix} e^{i\phi_1^B} & e^{i\phi_1^B} & e^{i\phi_1^B} & e^{i\phi_1^B} \\ e^{i\phi_2^B} & e^{i\phi_2^B} & -e^{i\phi_2^B} & -e^{i\phi_2^B} \\ e^{i\phi_3^B} & -e^{i\phi_3^B} & e^{i\phi_3^B} & -e^{i\phi_3^B} \\ e^{i\phi_4^B} & -e^{i\phi_4^B} & -e^{i\phi_4^B} & e^{i\phi_4^B} \end{bmatrix}, \quad (9)$$

where  $\phi_k^B$  is the phase applied in the core mode  $k$  at the measurement side. After applying the phases, we conclude the projective measurement using a final DEMUX (denoted DEMUX<sub>3</sub>), to send the outcomes of MBS<sub>1</sub> to four single-photon detectors (SPD). The detectors are triggered commercial single-photon detection modules, configured with 5-ns detection gates and 10% of detection efficiency. The detection counts are recorded by the FPGA unit. The measurement corresponding to the above procedure is the rank-1 projective measurement given by the states

$$\begin{aligned} |\alpha_1\rangle &= \frac{1}{2}(e^{i\phi_1^B}|1\rangle + e^{i\phi_2^B}|2\rangle + e^{i\phi_3^B}|3\rangle + e^{i\phi_4^B}|4\rangle), \\ |\alpha_2\rangle &= \frac{1}{2}(e^{i\phi_1^B}|1\rangle + e^{i\phi_2^B}|2\rangle - e^{i\phi_3^B}|3\rangle - e^{i\phi_4^B}|4\rangle), \\ |\alpha_3\rangle &= \frac{1}{2}(e^{i\phi_1^B}|1\rangle - e^{i\phi_2^B}|2\rangle + e^{i\phi_3^B}|3\rangle - e^{i\phi_4^B}|4\rangle), \\ |\alpha_4\rangle &= \frac{1}{2}(e^{i\phi_1^B}|1\rangle - e^{i\phi_2^B}|2\rangle - e^{i\phi_3^B}|3\rangle + e^{i\phi_4^B}|4\rangle). \end{aligned} \quad (10)$$

That is, photon detection in path  $k$  corresponds to the measurement outcome associated with  $|\alpha_k\rangle$ .

Therefore, in our experiment, we can prepare the state of Eq. (8) and measure it in the basis defined by the

orthogonal states of Eq. (10). The PMs, DEMUXs, and MBSs present an average insertion loss of 2.05 dB, 0.4 dB, and 0.2 dB, respectively, contributing to a total 3.66 dB of insertion loss for the entire measurement stage. Fiber-based polarization controllers (PCs) (not shown for the sake of simplicity) are used in each path to guarantee the indistinguishability of the core modes, such that there is no path information available to compromise the visibility of the interferometer [64,65]. These PCs are placed at the input of DEMUX<sub>2</sub> and are calibrated before each experimental round, keeping the polarization aligned for hours in the laboratory environment.

The most destructive disturbance in the setup is a time-dependent phase noise between the different arms of the interferometer, which arises due to thermal and mechanical fluctuations in the SMFs. For the preparation stage, the total applied phase is modeled considering that  $\phi_k^A = \phi_k^n + \phi_k^c + \phi_k^s$ . Here,  $\phi_k^n$  represents the phase noise,  $\phi_k^c$  the phase-noise suppressor, which we control by a continuous low-speed voltage signal, and  $\phi_k^s$  the phase used to prepare the desired state, which we control by a high-speed voltage. Both voltages are controlled by the FPGA unit through a power driver (for more details, see the Appendix). The phase noise is canceled out by controlling  $\phi_k^c$ : a control algorithm in the FPGA sets  $\tau_k = 1$  and  $\phi_k^s = 0$ , ideally preparing  $|\chi^{\max}\rangle = \frac{1}{2}(|1\rangle + |2\rangle + |3\rangle + |4\rangle)$  and, simultaneously, sets  $\phi_k^B = 0$ , ideally measuring in the basis  $A$  of Eq. (12). With these settings, if the phase noise is null, the photon always arrives at SPD<sub>1</sub>, that is,  $p_1 = |\langle\alpha_1|\chi^{\max}\rangle|^2 = 1$ . Similarly, by preparing the state  $|\chi^{\min}\rangle = \frac{1}{2}(|1\rangle + |2\rangle - |3\rangle - |4\rangle)$ , the expected probability of photon detection at SPD<sub>1</sub> is  $p_1 = |\langle\alpha_1|\chi^{\min}\rangle|^2 = 0$ . Therefore, we expect maximal counts for  $|\chi^{\max}\rangle$  and minimal counts for  $|\chi^{\min}\rangle$ . By collecting data at SPD<sub>1</sub> for these two settings, we can calculate the setup visibility, defined as

$$V_{\text{SPD}_1} = \frac{\text{SC}_{\text{SPD}_1}^{\max} - \text{SC}_{\text{SPD}_1}^{\min}}{\text{SC}_{\text{SPD}_1}^{\max} + \text{SC}_{\text{SPD}_1}^{\min}}, \quad (11)$$

where SC<sub>SPD<sub>1</sub></sub><sup>max</sup> (SC<sub>SPD<sub>1</sub></sub><sup>min</sup>) is the number of accumulated single counts of SPD<sub>1</sub> given the state preparation  $|\chi^{\max}\rangle$  ( $|\chi^{\min}\rangle$ ). The algorithm sets a threshold visibility  $V_{\text{SPD}_1} = 99.7\%$  and adjusts the control phases  $\phi_k^c$  until this threshold is achieved. This algorithm is known as *perturb and observe maximum power point tracking* [66]. Once the threshold is reached (corresponding to  $\phi_k^c \approx -\phi_k^n$ ), the suppressor phase  $\phi_k^c$  is held to begin the experimental round and the experiment is performed using the fast-switching phases  $\phi_k^s$  and  $\phi_k^B$  for preparing and measuring the states in the protocol, respectively. To maintain high optical quality, the system defines an interval of 0.1 s for the experimental data collection, after which it calibrates  $\phi_k^c$  again to counteract the time-dependent phase noise. The FPGA unit

controls and synchronizes the preparation and measurement stages, both working at a repetition rate of 2 MHz, achieving around 60 000 detections during a time interval of 1 s.

The measurements, which we aim to certify, correspond to a pair of MUBs, which we choose such that they can be implemented in our setup using only phase modulation, without the need for amplitude modulation. Specifically, the two bases  $\{|a_i\rangle\}_{i=1}^4$  and  $\{|b_j\rangle\}_{j=1}^4$  are given by the columns of the matrices

$$A = \frac{1}{2} \begin{bmatrix} 1 & 1 & 1 & 1 \\ 1 & 1 & -1 & -1 \\ 1 & -1 & 1 & -1 \\ 1 & -1 & -1 & 1 \end{bmatrix}, \quad (12)$$

$$B = \frac{1}{2} \begin{bmatrix} -1 & -1 & -1 & -1 \\ 1 & 1 & -1 & -1 \\ 1 & -1 & 1 & -1 \\ 1 & -1 & -1 & 1 \end{bmatrix}. \quad (13)$$

According to Eq. (9),  $A$  can be performed by setting the phases  $\phi_k^B = 0$  for all  $k = 1, 2, 3, 4$ , while  $B$  can be performed by setting  $\phi_1^B = \pi$  and keeping the other phases equal to zero. In the QRAC protocol described above, Bob chooses the measurement basis  $A$  or  $B$  according to his input  $y$ . In our experiment, we perform this basis choice simply by changing  $\phi_1^B$ : when  $y = 1$ , we choose  $\phi_1^B = 0$  and when  $y = 2$ , we choose  $\phi_1^B = \pi$ .

The optimal state preparation for Alice's input  $i, j$  is the pure state [25]:

$$|\psi_{ij}\rangle = \frac{1}{\sqrt{3}}[|a_i\rangle + \text{sgn}(\langle a_i|b_j\rangle)|b_j\rangle], \quad (14)$$

which we can produce according to Eq. (8). The QRAC protocol is then carried out by randomly preparing the 16 different states  $|\psi_{ij}\rangle$  with  $i, j \in \{1, 2, 3, 4\}$ , randomly measuring them in the bases  $A$  or  $B$  and collecting the measurement statistics to estimate the average success probability in Eq. (2). The choices of states and measurements are implemented directly in the FPGA by resorting to a pseudorandom-number-generation algorithm.

## V. RESULTS

We present the recorded experimental data in two parts, corresponding to the success probabilities related to the measurements  $A$  and  $B$  of Eq. (2). In the experiment, data are accumulated over 565 s, recording a total of 32 628 502 detections, with an average experimental detection rate of 57 883 detections per second. Figure 3(a) contains the outcome probabilities for the interferometer's outcomes 1, 2, 3, and 4 for each state  $|\psi_{ij}\rangle$  upon measuring  $A$ . In Fig.

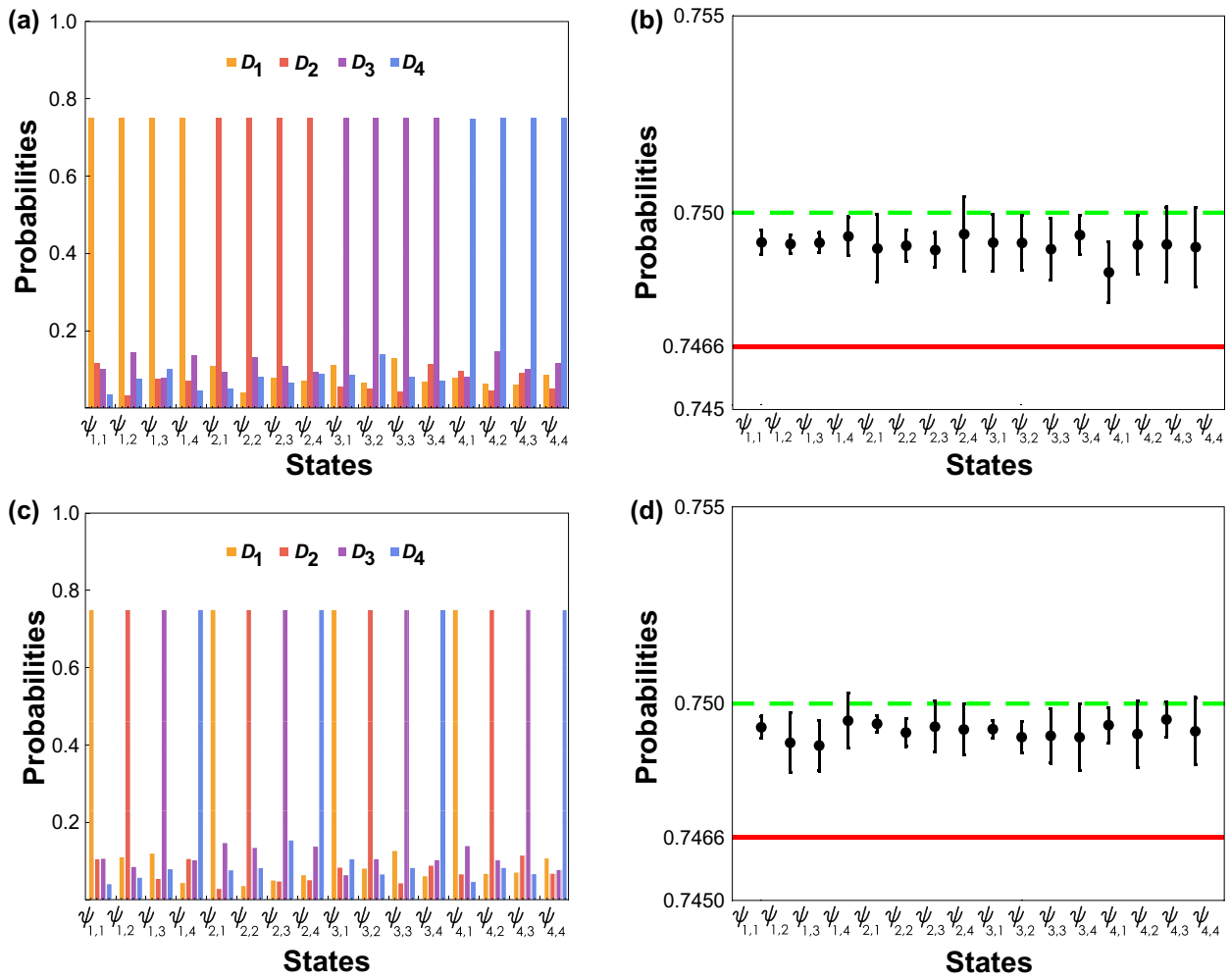


FIG. 3. (a),(c) The outcome probabilities of the measurements  $A$  and  $B$ , respectively, for each state  $|\psi_{ij}\rangle$ . (b),(d) The ASP for each state  $|\psi_{ij}\rangle$  upon measuring  $A$  and  $B$ , respectively. The green line corresponds to the optimal ASP  $\bar{p} = 0.75$ , while the red line corresponds to the minimal ASP such that the most demanding quantity,  $\eta^*$ , can be self-tested.

3(b), we show the ASP for each state  $|\psi_{ij}\rangle$  upon measuring  $A$ . On average, we observe an ASP of  $\bar{p}_A = 0.7491 \pm 0.0002$  for this measurement, where the error is calculated using the Poissonian distribution for the number of photon detections. The analogous data for the measurement  $B$  are depicted in Figs. 3(c) and 3(d), yielding an ASP of  $\bar{p}_B = 0.7493 \pm 0.0001$  in this case.

Putting the above values together, the overall ASP is  $\bar{p} = 0.7492 \pm 0.0001$ . Using this result and Gaussian error propagation, from Eq. (3) we obtain that  $H_S(A, B) \geq 3.991 \pm 0.001$ . From Eq. (4), we obtain that  $N(A) \geq 3.957 \pm 0.006$ . These two results, together, self-test the fact that the measurements are close to a pair of MUBs [ $H_S(A, B) = 4$  and  $N(A) = 4$ ].

Concerning the operational quantities, from Eq. (5), we obtain  $\eta^* \leq 0.80 \pm 0.01$ . Therefore, we certify a non-trivial bound on the critical visibility of our measurements at which they become compatible. This confirms that the measurements used in the experiment are indeed

incompatible and therefore will be useful in future Bell and steering experiments [58].

Lastly, from Eq. (6), we can bound the entropic uncertainty:  $H(A)_\rho + H(B)_\rho \geq 1.25 \pm 0.05$ . That is, we obtain a minimal entropy that can be extracted from the outcomes of our measurements on *any* quantum state. This can be used for secure random-number generation or quantum key distribution protocols.

## VI. CONCLUSIONS

With the development of quantum technologies, there is a current need for certification schemes for preparing high-dimensional quantum states and measurements. Since self-testing methods in nonlocal scenarios are complicated both in theory and practice, recently proposed methods for self-testing quantum devices in the prepare-and-measure scenario become relevant. In this work, we

demonstrate the viability of adopting such type of protocols in higher dimensions to validate the proper functioning of quantum devices built with modern SDM technology. Specifically, we self-test the proper implementation of measurements corresponding to mutually unbiased bases in dimension  $d = 4$ . This technology can be scaled to perform quantum-information processing protocols up to dimension 32 [67–69].

Our results show that SDM is an advantageous platform for high-dimensional quantum-information processing, achieving an exceptionally high optical quality with visibilities greater than 99%. While experiments implementing the same protocol have previously been performed [31–33], our technique allows us not only to certify the quantum advantage in random access coding but to self-test the measurements under the dimension assumption, as well as to certify their level of incompatibility and the amount of randomness that can be extracted from their outcomes. These results are of practical relevance for future experiments relying on this technology, since mutually unbiased measurements lie at the core of several quantum-information protocols.

## ACKNOWLEDGMENTS

This work was supported by the Fondo Nacional de Desarrollo Científico y Tecnológico (FONDECYT) under Grants No. 1190933 and No. 1200859 and by the National Agency of Research and Development (ANID) Millennium Science Initiative program ICN17\_012. J.C. acknowledges support from ANID/REC/PAI77190088. M.F. acknowledges support from the Polish National Science Center (NCN), under Grant No. Sonata UMO-2014/14/E/ST2/00020, from the project of the Polish National Agency for Academic Exchange “International scholarship exchange of PhD candidates and academic staff,” Project No. POWR.03.03.00-IP.08-00-P13/18, from the European Research Council (ERC) Advanced Grant (AdG) “Certification of quantum technologies” project (CERQUTE), from the Government of Spain (FIS2020-TRANQI and Severo Ochoa CEX2019-000910-S), and from the Fundació Cellex, Fundació Mir-Puig, Generalitat de Catalunya (CERCA, AGAUR SGR 1381).

## APPENDIX: EXPERIMENTAL DETAILS OF THE INNER WORKING OF THE FPGA

The FPGA electronic unit used in our experiment is based on the scheme shown in Fig. 4. Inside the FPGA, there are the following six main modules: the central processing unit (CPU), detection control (DC), phase-noise control (PNC), the preparation stage (PS), the measurement stage (MS), and a pseudorandom-number generator (RNG). The CPU module connects the FPGA unit with the user, synchronizes all internal modules (including a trigger for the single-photon source), controls the PNC

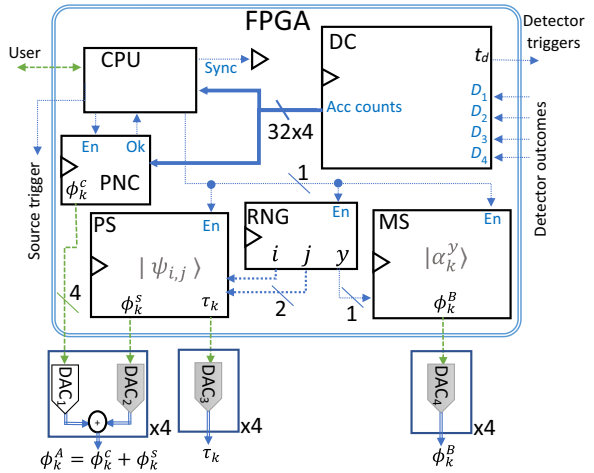


FIG. 4. The electronic diagram inside the FPGA.

module process, and executes the QRAC protocol. The RNG module is configured to randomly select the values of the three variables,  $i$ ,  $j$ , and  $y$ , from a preset pseudorandom sequence. Note that the variables  $i$  and  $j$  are two bits each, while  $y$  is a single bit. The variables  $i$  and  $j$  are used by the PS module to prepare the desired state, while the MS module uses the variable  $y$  to select the corresponding measurement basis. The DC module synchronizes the four SPDs with the trigger signal, records their detection counts, and saves these data in four registers of 32 bits. The experimental probabilities are calculated from these data and they also provide the probability  $p_1$  to the PNC module. The PNC module then uses these data to disturb the control phases  $\phi_k^c$  [66].

As described in the main text, if the visibility is greater than a threshold, the phase-noise control ( $\phi_k^c$ ) is fixed to the values found and then the PS and MS modules are enabled. These modules prepare the required phases and transmissions based on the three variables ( $i$ ,  $j$ , and  $y$ ) that correspond to preset voltages to prepare the state and measurement basis needed in this protocol. The modules work at a repetition rate of 2 MHz. After 0.1 s of experimental run, the PS and MS modules are disabled in order for the PNC module to check visibility again.

The digital signals from the FPGA unit are converted using two different digital-to-analog converters (DACS) (see Fig. 4). Here, DAC<sub>1</sub> is 12-bits serial and the others are 4-bits parallel for high speeds. Note that four drivers are required for each set of phases ( $\phi_k^A$  and  $\phi_k^B$ ) and transmissions ( $\tau_k$ ).

- [1] P. W. Shor, in *Proceedings 35th Annual Symposium on Foundations of Computer Science* (IEEE, Santa Fe, NM, USA, 1994), p. 124.
- [2] R. P. Feynman, Simulating physics with computers, *Int. J. Theor. Phys.* **21**, 467 (1982).

- [3] C. H. Bennett and G. Brassard, in *Proceedings Of The IEEE International Conference On Computers, Systems And Signal Processing, Bangalore, India* (IEEE, New York, 1984), p. 175.
- [4] A. K. Ekert, Quantum Cryptography Based on Bell's Theorem, *Phys. Rev. Lett.* **67**, 661 (1991).
- [5] A. Acín, N. Brunner, N. Gisin, S. Massar, S. Pironio, and V. Scarani, Device-Independent Security of Quantum Cryptography against Collective Attacks, *Phys. Rev. Lett.* **98**, 230501 (2007).
- [6] R. Gallego, N. Brunner, C. Hadley, and A. Acín, Device-Independent Tests of Classical and Quantum Dimensions, *Phys. Rev. Lett.* **105**, 230501 (2010).
- [7] J.-D. Bancal, N. Gisin, Y.-C. Liang, and S. Pironio, Device-Independent Witnesses of Genuine Multipartite Entanglement, *Phys. Rev. Lett.* **106**, 250404 (2011).
- [8] R. Rabelo, L. Y. Zhi, and V. Scarani, Device-Independent Bounds for Hardy's Experiment, *Phys. Rev. Lett.* **109**, 180401 (2012).
- [9] T. H. Yang and M. Navascués, Robust self-testing of unknown quantum systems into any entangled two-qubit states, *Phys. Rev. A* **87**, 050102(R) (2013).
- [10] M. Ho, J.-D. Bancal, and V. Scarani, Device-independent certification of the teleportation of a qubit, *Phys. Rev. A* **88**, 052318 (2013).
- [11] E. S. Gómez, S. Gómez, P. González, G. Cañas, J. F. Barra, A. Delgado, G. B. Xavier, A. Cabello, M. Kleinmann, T. Vértesi, and G. Lima, Device-Independent Certification of a Nonprojective Qubit Measurement, *Phys. Rev. Lett.* **117**, 260401 (2016).
- [12] S. Gómez, A. Mattar, I. Machuca, E. S. Gómez, D. Cavalcanti, O. J. Fariás, A. Acín, and G. Lima, Experimental investigation of partially entangled states for device-independent randomness generation and self-testing protocols, *Phys. Rev. A* **99**, 032108 (2019).
- [13] I. Šupić and J. Bowles, Self-testing of quantum systems: A review, *Quantum* **4**, 337 (2020).
- [14] J. Kaniewski, I. Šupić, J. Tura, F. Baccari, A. Salavrakos, and R. Augusiak, Maximal nonlocality from maximal entanglement and mutually unbiased bases, and self-testing of two-qutrit quantum systems, *Quantum* **3**, 198 (2019).
- [15] S. Sarkar, D. Saha, J. Kaniewski, and R. Augusiak, Self-testing quantum systems of arbitrary local dimension with minimal number of measurements, [arXiv:1909.12722](https://arxiv.org/abs/1909.12722) (2019).
- [16] D. Kaszlikowski, P. Gnaciński, M. Żukowski, W. Miklaszewski, and A. Zeilinger, Violations of Local Realism by Two Entangled  $N$ -Dimensional Systems Are Stronger than for Two Qubits, *Phys. Rev. Lett.* **85**, 4418 (2000).
- [17] M. Araújo, F. Costa, and Č. Brukner, Computational Advantage from Quantum-Controlled Ordering of Gates, *Phys. Rev. Lett.* **113**, 250402 (2014).
- [18] D. Martínez, A. Tavakoli, M. Casanova, G. Cañas, B. Marques, and G. Lima, High-Dimensional Quantum Communication Complexity beyond Strategies Based on Bell's Theorem, *Phys. Rev. Lett.* **121**, 150504 (2018).
- [19] J. Cariñe, G. Cañas, P. Skrzypczyk, I. Šupić, N. Guerrero, T. Garcia, L. Pereira, M. A. S. Prosser, G. B. Xavier, A. Delgado, S. P. Walborn, D. Cavalcanti, and G. Lima, Multi-core fiber integrated multi-port beam splitters for quantum information processing, *Optica* **7**, 542 (2020).
- [20] T. Van Himbeeck, E. Woodhead, N. J. Cerf, R. García-Patrón, and S. Pironio, Semi-device-independent framework based on natural physical assumptions, *Quantum* **1**, 33 (2017).
- [21] J. B. Brask, A. Martin, W. Esposito, R. Houlmann, J. Bowles, H. Zbinden, and N. Brunner, Megahertz-Rate Semi-Device-Independent Quantum Random Number Generators Based on Unambiguous State Discrimination, *Phys. Rev. Appl.* **7**, 054018 (2017).
- [22] M. Hendrych, R. Gallego, M. Mićuda, N. Brunner, A. Acín, and J. P. Torres, Experimental estimation of the dimension of classical and quantum systems, *Nat. Phys.* **8**, 588 (2012).
- [23] J. Ahrens, P. Badziag, A. Cabello, and M. Bourennane, Experimental device-independent tests of classical and quantum dimensions, *Nat. Phys.* **8**, 592 (2012).
- [24] V. D'Ambrosio, F. Bisesto, F. Sciarrino, J. F. Barra, G. Lima, and A. Cabello, Device-Independent Certification of High-Dimensional Quantum Systems, *Phys. Rev. Lett.* **112**, 140503 (2014).
- [25] M. Farkas and J. Kaniewski, Self-testing mutually unbiased bases in the prepare-and-measure scenario, *Phys. Rev. A* **99**, 032316 (2019).
- [26] I. D. Ivanovic, Geometrical description of quantal state determination, *J. Phys. A: Math. Gen.* **14**, 3241 (1981).
- [27] G. Lima, L. Neves, R. Guzmán, E. S. Gómez, W. A. T. Nogueira, A. Delgado, A. Vargas, and C. Saavedra, Experimental quantum tomography of photonic qudits via mutually unbiased basis, *Opt. Express* **19**, 3542 (2011).
- [28] H. Maassen and J. B. M. Uffink, Generalized Entropic Uncertainty Relations, *Phys. Rev. Lett.* **60**, 1103 (1988).
- [29] T. Durt, B. Englert, I. Bengtsson, and K. Życzkowski, On mutually unbiased bases, *Int. J. Quantum Inf.* **8**, 535 (2010).
- [30] G. B. Xavier and G. Lima, Quantum information processing with space-division multiplexing optical fibres, *Commun. Phys.* **3**, 9 (2020).
- [31] A. Tavakoli, A. Hameedi, B. Marques, and M. Bourennane, Quantum Random Access Codes Using Single  $d$ -Level Systems, *Phys. Rev. Lett.* **114**, 170502 (2015).
- [32] M. J. Kewming, S. Shrapnel, A. G. White, and J. Romero, Hiding Ignorance Using High Dimensions, *Phys. Rev. Lett.* **124**, 250401 (2020).
- [33] E. A. Aguilar, M. Farkas, D. Martínez, M. Alvarado, J. Cariñe, G. B. Xavier, J. F. Barra, G. Cañas, M. Pawłowski, and G. Lima, Certifying an Irreducible 1024-Dimensional Photonic State Using Refined Dimension Witnesses, *Phys. Rev. Lett.* **120**, 230503 (2018).
- [34] P. Mironowicz, A. Tavakoli, A. Hameedi, B. Marques, M. Pawłowski, and M. Bourennane, Increased certification of semi-device independent random numbers using many inputs and more post-processing, *New J. Phys.* **18**, 065004 (2016).
- [35] M. Pawłowski and N. Brunner, Semi-device-independent security of one-way quantum key distribution, *Phys. Rev. A* **84**, 010302(R) (2011).
- [36] T. Heinosaari, J. Kiukas, and D. Reitzner, Noise robustness of the incompatibility of quantum measurements, *Phys. Rev. A* **92**, 022115 (2015).
- [37] M. T. Quintino, T. Vértesi, and N. Brunner, Joint Measurability, Einstein-Podolsky-Rosen Steering, and Bell Nonlocality, *Phys. Rev. Lett.* **113**, 160402 (2014).

- [38] P. J. Coles, M. Berta, M. Tomamichel, and S. Wehner, Entropic uncertainty relations and their applications, *Rev. Mod. Phys.* **89**, 015002 (2017).
- [39] Z. Pan, K.-K. Wong, and T.-S. Ng, Generalized multiuser orthogonal space-division multiplexing, *IEEE Trans. Wireless Commun.* **3**, 1969 (2004).
- [40] D. J. Richardson, J. M. Fini, and L. E. Nelson, Space-division multiplexing in optical fibres, *Nat. Photonics* **7**, 354 (2013).
- [41] P. Sillard, M. Bigot-Astruc, and D. Molin, Few-mode fibers for mode-division-multiplexed systems, *J. Lightwave Technol.* **32**, 2824 (2014).
- [42] G. Rademacher, R. S. Luís, B. J. Puttnam, T. A. Eriksson, R. Ryf, E. Agrell, R. Maruyama, K. Aikawa, Y. Awaji, H. Furukawa, and N. Wada, High capacity transmission with few-mode fibers, *J. Lightwave Technol.* **37**, 425 (2019).
- [43] K. Kitayama and N. Diamantopoulos, Few-mode optical fibers: Original motivation and recent progress, *IEEE Commun. Mag.* **55**, 163 (2017).
- [44] C. Brunet, B. Ung, L. Wang, Y. Messaddeq, S. LaRochelle, and L. A. Rusch, Design of a family of ring-core fibers for OAM transmission studies, *Opt. Express* **23**, 10553 (2015).
- [45] S. Inao, T. Sato, S. Sentsui, T. Kuroha, and Y. Nishimura, in *Optical Fiber Communication*, 1979 OSA Technical Digest Series (Optical Society of America, Washington, D.C., 1979), paper WB1.
- [46] K. Saitoh and S. Matsuo, Multicore fiber technology, *J. Lightwave Technol.* **34**, 55 (2016).
- [47] L. Zhu, G. Zhu, A. Wang, L. Wang, J. Ai, S. Chen, C. Du, J. Liu, S. Yu, and J. Wang, 18 km low-crosstalk OAM + WDM transmission with 224 individual channels enabled by a ring-core fiber with large high-order mode group separation, *Opt. Lett.* **43**, 1890 (2018).
- [48] T. A. Birks, I. Gris-Sánchez, S. Yerolatsitis, S. G. Leon-Saval, and R. R. Thomson, The photonic lantern, *Adv. Opt. Photon.* **7**, 107 (2015).
- [49] G. C. G. Berkhout, M. P. J. Lavery, J. Courtial, M. W. Beijersbergen, and M. J. Padgett, Efficient Sorting of Orbital Angular Momentum States of Light, *Phys. Rev. Lett.* **105**, 153601 (2010).
- [50] X. Zeng, Y. Li, L. Feng, S. Wu, C. Yang, W. Li, W. Tong, and J. Wu, All-fiber orbital angular momentum mode multiplexer based on a mode-selective photonic lantern and a mode polarization controller, *Opt. Lett.* **43**, 4779 (2018).
- [51] K. Watanabe, T. Saito, K. Imamura, and M. Shiino, in *2012 17th Opto-Electronics and Communications Conference* (IEEE, Busan, 2012), p. 475.
- [52] Y. Tottori, T. Kobayashi, and M. Watanabe, Low loss optical connection module for seven-core multicore fiber and seven single-mode fibers, *IEEE Photonics Technol. Lett.* **24**, 1926 (2012).
- [53] L. Gan, R. Wang, D. Liu, L. Duan, S. Liu, S. Fu, B. Li, Z. Feng, H. Wei, W. Tong, P. Shum, and M. Tang, Spatial-division multiplexed Mach-Zehnder interferometers in heterogeneous multicore fiber for multiparameter measurement, *IEEE Photonics J.* **8**, 1 (2016).
- [54] J. F. Dynes, S. J. Kindness, S. W.-B. Tam, A. Plews, A. W. Sharpe, M. Lucamarini, B. Fröhlich, Z. L. Yuan, R. V. Penty, and A. J. Shields, Quantum key distribution over multicore fiber, *Opt. Express* **24**, 8081 (2016).
- [55] G. Cañas, N. Vera, J. Cariñe, P. González, J. Cardenas, P. W. R. Connolly, A. Przysiezna, E. S. Gómez, M. Figueroa, G. Vallone, P. Villoresi, T. F. da Silva, G. B. Xavier, and G. Lima, High-dimensional decoy-state quantum key distribution over multicore telecommunication fibers, *Phys. Rev. A* **96**, 022317 (2017).
- [56] Y. Ding, D. Bacco, K. Dalgaard, X. Cai, X. Zhou, K. Rotwitt, and L. K. Oxenløwe, High-dimensional quantum key distribution based on multicore fiber using silicon photonic integrated circuits, *npj Quantum Inf.* **3**, 25 (2017).
- [57] H. J. Lee, S.-K. Choi, and H. S. Park, Experimental demonstration of four-dimensional photonic spatial entanglement between multi-core optical fibres, *Sci. Rep.* **7**, 4302 (2017).
- [58] E. S. Gómez, S. Gómez, I. Machuca, A. Cabello, S. Pádua, S. P. Walborn, and G. Lima, Multi-dimensional entanglement generation with multi-core optical fibers, *arXiv:2005.07847* (2020).
- [59] L. Cui, J. Su, X. Li, and Z. Y. Ou, Distribution of entangled photon pairs over few-mode fibers, *Sci. Rep.* **7**, 14954 (2017).
- [60] A. Sit, R. Fickler, F. Alsaiari, F. Bouchard, H. Larocque, P. Gregg, L. Yan, R. W. Boyd, S. Ramachandran, and E. Karimi, Quantum cryptography with structured photons through a vortex fiber, *Opt. Lett.* **43**, 4108 (2018).
- [61] H. Cao, S.-C. Gao, C. Zhang, J. Wang, D.-Y. He, B.-H. Liu, Z.-W. Zhou, Y.-J. Chen, Z.-H. Li, S.-Y. Yu, J. Romero, Y.-F. Huang, C.-F. Li, and G.-C. Guo, Distribution of high-dimensional orbital angular momentum entanglement over a 1 km few-mode fiber, *Optica* **7**, 232 (2020).
- [62] D. Cozzolino, E. Polino, M. Valeri, G. Carvacho, D. Bacco, N. Spagnolo, L. K. K. Oxenløwe, and F. Sciarrino, Air-core fiber distribution of hybrid vector vortex-polarization entangled states, *Adv. Photonics* **1**, 046005 (2019).
- [63] N. Gisin, G. Ribordy, W. Tittel, and H. Zbinden, Quantum cryptography, *Rev. Mod. Phys.* **74**, 145 (2002).
- [64] S. P. Walborn, M. O. Terra Cunha, S. Pádua, and C. H. Monken, Double-slit quantum eraser, *Phys. Rev. A* **65**, 033818 (2002).
- [65] F. A. Torres-Ruiz, G. Lima, A. Delgado, S. Pádua, and C. Saavedra, Decoherence in a double-slit quantum eraser, *Phys. Rev. A* **81**, 042104 (2010).
- [66] W. Liu, C. Liu, L. Ma, Y. Lin, and J. Ma, Maximum power point tracking of photovoltaic generation based on forecasting model, *J. Softw.* **8**, 2569 (2013).
- [67] K. Takenaga, S. Matsuo, K. Saitoh, T. Morioka, and Y. Miyamoto, in *Optical Fiber Communications Conference and Exhibition (OFC)* (Optical Society of America, Anaheim, CA, 2016), p. 1.
- [68] B. J. Puttnam, R. S. Luís, G. Rademacher, A. Alfredsson, W. Klaus, J. Sakaguchi, Y. Awaji, E. Agrell, and N. Wada, Characteristics of homogeneous multi-core fibers for SDM transmission, *APL Photonics* **4**, 022804 (2019).
- [69] T. Mizuno, K. Shibahara, F. Ye, Y. Sasaki, Y. Amma, K. Takenaga, Y. Jung, K. Pulverer, H. Ono, Y. Abe, M. Yamada, K. Saitoh, S. Matsuo, K. Aikawa, M. Bohn, D. J. Richardson, Y. Miyamoto, and T. Morioka, Long-haul dense space-division multiplexed transmission over low-crosstalk heterogeneous 32-core transmission line using a partial recirculating loop system, *J. Lightwave Technol.* **35**, 488 (2017).